Interaction-induced quantum anomalous Hall phase in (111) bilayer of $LaCoO_3$

Yilin Wang,[1] Zhijun Wang,[1] Zhong Fang,[1,2] and Xi Dai[1,2]

[1]*Beijing National Laboratory for Condensed Matter Physics, and Institute of Physics, Chinese Academy of Sciences, Beijing 100190, China*

[2]*Collaborative Innovation Center of Quantum Matter, Beijing 100190, China*

(Received 13 October 2014; revised manuscript received 10 March 2015; published 25 March 2015)

In the present paper, the Gutzwiller density functional theory (LDA+G) has been applied to study the bilayer system of $LaCoO_3$ grown along the (111) direction on $SrTiO_3$. The LDA calculations show that there are two nearly flat bands located at the top and bottom of e_g bands of Co atoms with the Fermi level crossing the lower one. After including both the spin-orbit coupling and the Coulomb interaction in the LDA+G method, we find that the interplay between spin-orbit coupling and Coulomb interaction stabilizes a very robust ferromagnetic insulator phase with the nonzero Chern number indicating the possibility of realizing the quantum anomalous Hall effect in this system.

DOI: 10.1103/PhysRevB.91.125139 PACS number(s): 73.21.−b, 71.27.+a, 73.43.−f

I. INTRODUCTION

Searching for topologically nontrivial phases [1,2] in realistic material systems is one of the fast developing research fields in condensed matter physics. Recently, transition metal oxides (TMOs) have been proposed [3] as a potential platform for topological materials due to many of its advantages compared to the previously found topological compounds, such as HgTe [4–6] and Bi_2Se_3 family compounds [7–9]. First of all, oxides are chemically much more stable when exposing in the air, which makes it more attractive for potential applications. Secondly, the relatively strong Coulomb interaction among the electrons in 3*d* orbitals generates fruitful many-body physics in TMOs and provides a tantalizing field for the search of topological materials. Finally, the rapid development of the techniques for the heterostructure growth of TMOs [10–12] paves a completely new path for realizing topological phases in condensed matter systems by material design.

D. Xiao *et al.* [3] first pointed out that the (111) bilayer heterostructure of perovskite TMOs can be viewed as a buckled honeycomb lattice and has "natively" inverted band structure, which is very similar to the situation in graphene [13]. Based on the tight-binding (TB) and the first-principles calculations of (111) bilayer heterostructure of TMOs, they found that there are two nearly flat bands at the top and bottom of the e_g bands of TM ions, together with another two bands with nearly linear dispersion forming a similar Dirac point at K point. The appearance of both flat bands and Dirac points in this system can be ascribed to the special geometry effects of the honeycomb lattice, based on which several exotic topological states can be designed. The first one is to open a semiconductor gap at the Dirac point by spin-orbit coupling (SOC) leading to quantum spin Hall effect. Because the sizable strength of SOC is required in this proposal, the typical realistic system proposed in Ref. [3] is the $LaAlO_3/LaAuO_3/LaAlO_3$ heterostructure, which is still very difficult to grow experimentally so far. The second proposal in this field is to realize the quantum anomalous Hall effect (QAHE) in the (111) bilayer of 3*d* TMOs [14–17], which is experimentally much more feasible than the 4*d* or 5*d* TMOs. Although the SOC strength is about one order smaller than that of 4*d* or 5*d* TMOs, the strong Coulomb interaction can help to stabilize the topologically nontrivial phases. Recently, the similar heterostructure has been made, but unfortunately the ground state is found to be antiferromagnetic (AFM) [18].

In this paper, we propose another bilayer heterostructure of 3*d* TMO, $LaCoO_3$, grown along the (111) direction on $SrTiO_3$, as a promising candidate to realize QAHE, which has the following advantages: (1) comparing with 4*d* and 5*d* TMOs, $LaCoO_3$ is more accessible and its thin film is not difficult to synthesize, (2) the lower flat band in the heterostructure leads to a sharp peak of density of states around the Fermi level which induces a strong Stoner instability towards the ferromagnetic (FM) insulator phase, (3) although the bare SOC strength is quite small, it can be largely enhanced by strong Coulomb interaction among 3*d* electrons, (4) with both large enough exchange splitting and modified SOC induced by strong correlation effects, the system falls into a semiconductor state under FM order with a nonzero total Chern number.

II. METHOD

$LaCoO_3$ is a typical material with its band structure strongly modified by correlation effects. In this work, the Gutzwiller density functional theory (LDA+G) [19–22] is used to calculate the ground states and quasiparticle band structures of its bulk phase and heterostructure. The LDA part of the calculations was done with the Vienna Ab-initio Simulation Package (VASP) [23] with the projector augmented-wave (PAW) pseudopotential [24,25] and Perdew-Burke-Ernzerhof parametrization of the generalized gradient approximation (GGA-PBE) exchange-correlation functionals [26]. The energy cutoff of the plane-wave basis is set to be 400 eV, and a Γ-centered $11 \times 11 \times 11$ K-point grid for the bulk and $8 \times 8 \times 1$ for the heterostructure has been chosen, respectively.

In the Gutzwiller part, we solve a Hamiltonian in the Wannier representation, which reads

$$H = \sum_{ij,\alpha\beta\sigma} \left(t^{dd}_{ij,\alpha\beta\sigma} d^\dagger_{\alpha\sigma} d_{\beta\sigma} + t^{pp}_{ij,\alpha\beta\sigma} p^\dagger_{\alpha\sigma} p_{\beta\sigma} + t^{dp}_{ij,\alpha\beta\sigma} d^\dagger_{\alpha\sigma} p_{\beta\sigma} + t^{pd}_{ij,\alpha\beta\sigma} p^\dagger_{\alpha\sigma} d_{\beta\sigma} \right) + \frac{1}{2} \sum_{i,\alpha\beta\gamma\delta\sigma\sigma'} U_{\alpha\sigma,\beta\sigma',\gamma\sigma,\delta\sigma'} d^\dagger_{\alpha\sigma} \times d^\dagger_{\beta\sigma'} d_{\delta\sigma'} d_{\gamma\sigma} - \sum_{i,\alpha\sigma} \bar{U} \left(n_d - \frac{1}{2} \right) d^\dagger_{\alpha\sigma} d_{\alpha\sigma}, \quad (1)$$

where i,j is the site index, $\alpha,\beta,\gamma,\delta$ is the Wannier orbital index, and σ,σ' is the spin index.

The first two lines of Eq. (1) describing a d-p TB Hamiltonian consists of Co $3d$ orbitals and O $2p$ orbitals, which are constructed from the non-SOC LDA calculation by the maximally localized Wannier functions (MLWF) method [27] implemented in the WANNIER90 [28] package.

The third line of Eq. (1) describes the local atomic Coulomb interaction for Co $3d$ orbitals. We assume the spherical symmetry for the Coulomb interaction in the $LaCoO_3$ solid and use a full interaction tensor $U_{\alpha\sigma,\beta\sigma',\gamma\sigma,\delta\sigma'}$ for the entire d shell [29,30]. We first write down the U tensor in the complex spherical harmonics basis $\phi_m = R_{3d}(r)Y_2^m$. In this basis, the U tensor is

$$U_{m_1\sigma,m_2\sigma',m_3\sigma,m_4\sigma'} = \delta_{m_1+m_2,m_3+m_4}\sum_k c_k^{m_1,m_3}c_k^{m_4,m_2}F^k, \quad (2)$$

where $k = 0,2,4$ for the d shell, $c_k^{m_1,m_3}$ is the Gaunt coefficient which has been exactly calculated and tabulated in Table 1.2 in Ref. [29], and F^0,F^2,F^4 are the three Slater integrals which are unknown. Thus, the full U tensor is parametrized by F^0,F^2,F^4, however, we take $F^4/F^2 = 0.625$ as an approximation with good accuracy for the d shell [31]. Then we transform it to the Wannier basis (the cubic spherical harmonics) by using the transformations:

$$\begin{aligned}
d_{xy} &= -\frac{i}{\sqrt{2}}(\phi_2 - \phi_{-2}),\\
d_{xz} &= -\frac{1}{\sqrt{2}}(\phi_1 - \phi_{-1}),\\
d_{yz} &= \frac{i}{\sqrt{2}}(\phi_1 + \phi_{-1}),\\
d_{x^2-y^2} &= \frac{1}{\sqrt{2}}(\phi_2 + \phi_{-2}),\\
d_{3z^2-r^2} &= \phi_0.
\end{aligned}$$

We don't follow the traditional definition of Coulomb interaction as $U_d = F^0$ and Hund's rule coupling as $J_H = \frac{1}{14}(F^2+F^4)$; instead, we define the Kanamori type U and J in the Wannier basis [30], where the intraorbital Coulomb interaction is $U = F^0 + \frac{4}{49}F^2 + \frac{4}{49}F^4$, and the Hund's rule coupling is orbital-dependent (anisotropic):

$$\begin{aligned}
J(d_{xy},d_{xz}) &= J(d_{xy},d_{yz}) = J(d_{xz},d_{yz})\\
&= J(d_{xz},d_{x^2-y^2}) = J(d_{yz},d_{x^2-y^2})\\
&= \tfrac{3}{49}F^2 + \tfrac{20}{441}F^4,\\
J(d_{xy},d_{3z^2-r^2}) &= J(d_{x^2-y^2},\\
d_{3z^2-r^2}) &= \tfrac{4}{49}F^2 + \tfrac{15}{441}F^4,\\
J(d_{xz},d_{3z^2-r^2}) &= J(d_{yz},d_{3z^2-r^2}) = \tfrac{1}{49}F^2 + \tfrac{30}{441}F^4,\\
J(d_{xy},d_{x^2-y^2}) &= \tfrac{35}{441}F^4.
\end{aligned}$$

We take all the terms of Hund's rule coupling into account in our calculations and define an average value of them as $J = \frac{5}{98}(F^2+F^4)$ for the convenience of discussing our results. Thus, given parameters F^0,F^2 or U,J, we can construct the full interaction U tensor.

The fourth line of Eq. (1) is the double-counting term [32] used to substract the correlation effect which has been considered in the LDA calculations. $\bar{U}$ is the average Coulomb interaction, which is defined as

$$\bar{U} = \frac{\sum_a U + \sum_{a<b}(U-2J_{a,b}) + \sum_{a<b}(U-3J_{a,b})}{M(2M-1)}, \quad (3)$$

where $1 \leqslant a,b \leqslant M$, M is the total number of orbitals (not including spin), U is the intraorbital Coulomb interaction, and $J_{a,b}$ is the Hund's rule coupling between orbitals a and b. n_d is the total occupancy of $3d$ orbitals for one Co site from the LDA calculations.

This Hamiltonian will be treated by the rotationally invariant Gutzwiller variational method introduced in detail in Refs. [19–22]. The Gutzwiller variational wave function $|G\rangle$ is constructed by applying a projector operator P to the noninteracting wave function $|0\rangle$ derived from the LDA calculation,

$$|G\rangle = P|0\rangle. \quad (4)$$

The projector operator is chosen as

$$P = \prod_i \left(\sum_\alpha \lambda_\alpha^i |\Gamma_\alpha^i\rangle\langle\Gamma_\alpha^i|\right), \quad (5)$$

where i is the site index, $|\Gamma\rangle$ is the atomic eigenstates, and λ_α are the Gutzwiller variational parameters, which can be determined by minimizing the total energy of the ground state.

III. RESULTS AND DISCUSSION

The bulk material of $LaCoO_3$ has very complicated electronic and spin state transitions [33–51]. At low enough temperature ($T < 50$ K), it is a semiconductor with low spin (LS) state. With the increasing of temperature, it undergoes a spin state transition to intermediate spin (IS) state around $T = 100$ K. When temperature $T > 500$ K, another transition from IS semiconductor to high spin (HS) metal will occur. However, we just focus on the zero-temperature ground state in our calculations. As shown in Fig. 1(a), the bulk $LaCoO_3$ has a distorted perovskite structure with the $R\bar{3}c$ (No. 167) space group [40,50], which contains two equivalent Co atoms in each unit cell. In our calculations, we take the lattice parameters for temperature $T = 5$ K from Ref. [40].

The LDA band structure is shown in Fig. 1(b). The e_g (blue) and t_{2g} (red) bands of Co atoms overlap and give a metallic ground state contradicting with the experimental results [37–39] which show semiconductor behavior. After considering the Coulomb interaction and the Hund's rule coupling in our LDA+G calculations, we get a semiconductor ground state when $U = 7.0$ eV and $J = 0.6$ eV, as shown in Fig. 1(c), which is in good agreement with both the experimental result [37–39] and the numerical result obtained by LDA+DMFT [50]. Comparing with the LDA band structure in Fig. 1(b), the Gutzwiller method modifies the bands in two ways: (1) renormalizes the effective crystal field splitting between t_{2g} and e_g orbitals; and (2) renormalizes the bandwidth of t_{2g} and e_g bands to be much narrower, as a result, opens a gap between them. We also obtain the partial density of states from the LDA and LDA+G calculations, which are plotted in

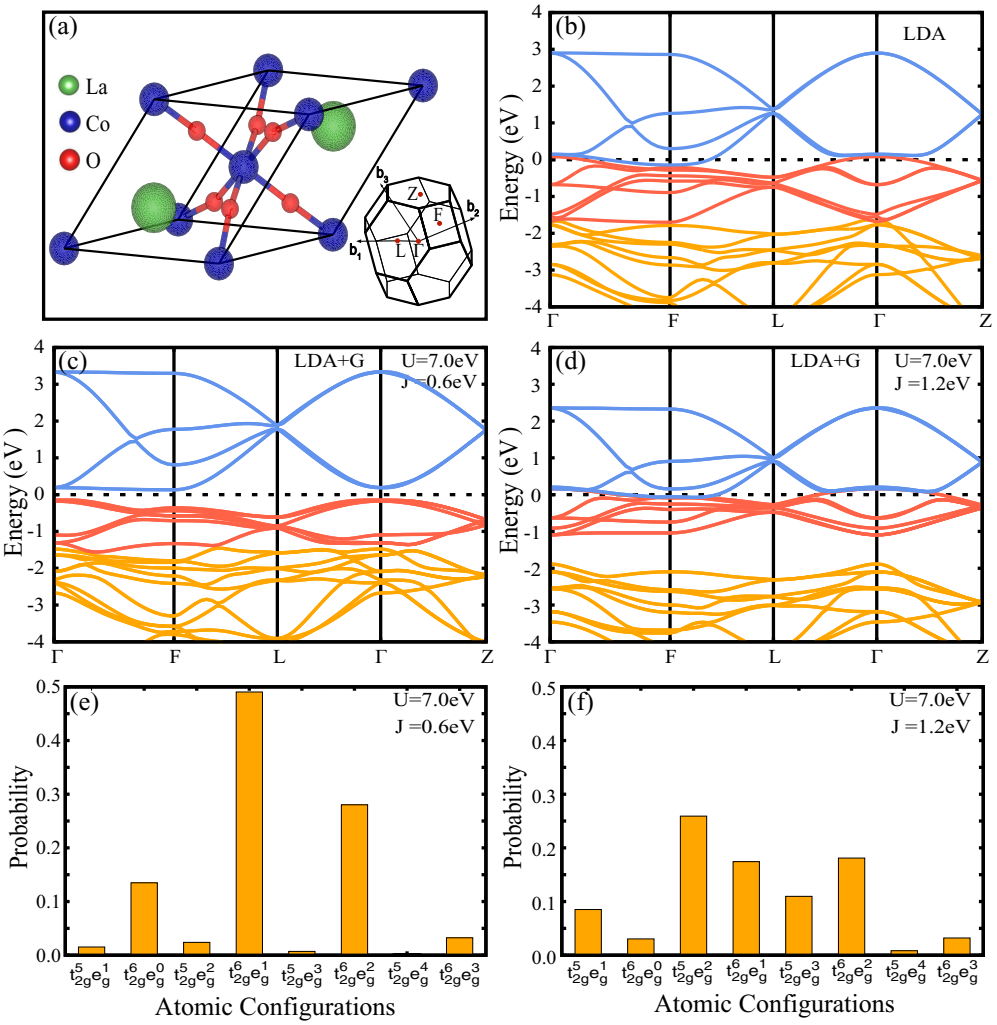

FIG. 1. (Color online) (a) The crystal structure of bulk $LaCoO_3$ with $R\bar{3}c$ (No. 167) space group and the corresponding Brillouin zone. (b) The band structures obtained from the LDA calculation. (c) and (d) The band structure obtained from the LDA+G calculations with the Coulomb interaction $U = 7.0$ eV, Hund's rule coupling $J = 0.6$ eV and $J = 1.2$ eV, respectively. (e) and (f) The corresponding probabilities of the atomic configurations $|I\rangle$ in the Gutzwiller wave function $|G\rangle$, $P_I = \langle G \mid I\rangle\langle I \mid G\rangle$ indicating the LS state for $J = 0.6$ eV and HS state for $J = 1.2$ eV.

Figs. 2(a) and 2(b). As we can see, the Co $3d$ bands strongly hybridize with O $2p$ bands; as a result, the calculated total occupation number of Co $3d$ orbitals, which is about 7.2, is larger than the nominal one, 6. From the quasiparticle band structure obtained by LDA+G, we can find that the band gap is between e_g and t_{2g} and it is a typical semiconductor with its band width renormalized by interaction about 80%. The corresponding probability of the atomic configurations $|I\rangle$ in the Gutzwiller ground state $|G\rangle$ can be calculated using the Gutzwiller wave function as $P_I = \langle G \mid I\rangle\langle I \mid G\rangle$, which are plotted in Fig. 1(e). There are mainly three configurations $t_{2g}^6e_g^0$,$t_{2g}^6e_g^1$,$t_{2g}^6e_g^2$ in the ground state indicating an LS state. Note that we call the spin states with fully filled t_{2g} orbitals (t_{2g}^6) the LS states, while those with some holes in the t_{2g} orbitals the HS states. To check how the Hund's rule coupling affects the spin states and the electronic structure, we increase it to $J = 1.2$ eV, and we get a metallic electronic structure with the HS state, as shown in Figs. 1(d) and 1(f). Locking between the metal-semiconductor transition with the spin state transition can be explained by the competition between the cubic crystal splitting and Hund's rule coupling. As a consequence, the increasing of Hund's rule coupling will strongly suppress the effective crystal splitting between t_{2g} and e_g orbitals leading to the disappearance of the semiconductor gap between them. We want to emphasize that this HS state is still a zero-temperature ground state, which is different with the temperature-induced IS and HS states in $LaCoO_3$.

We now turn to the heterostructure of $LaCoO_3$. The heterostructure of $LaCoO_3$ proposed in this paper is shown in Fig. 3(a), which contains two layers of Co and three layers of LaO_3 along the (111) direction on $SrTiO_3$. For one unit cell, the chemical formula is $Ti_{10}^{+4}Co_2^{+2.5}(LaO_3)_3^{-3}(SrO_3)_9^{-4}$. The heterostructure belongs to space group $P\bar{3}M1$ (No. 164) with an inversion center located at the O (0.5, 0.5, 0.5) site connecting two different layers of Co atoms, which form a buckled honeycomb lattice, as illustrated in Figs. 3(b)–3(d). The lattice parameter of $SrTiO_3$ is fixed to be 3.95 Å [3] and the internal atomic positions are optimized by LDA calculation using VASP.

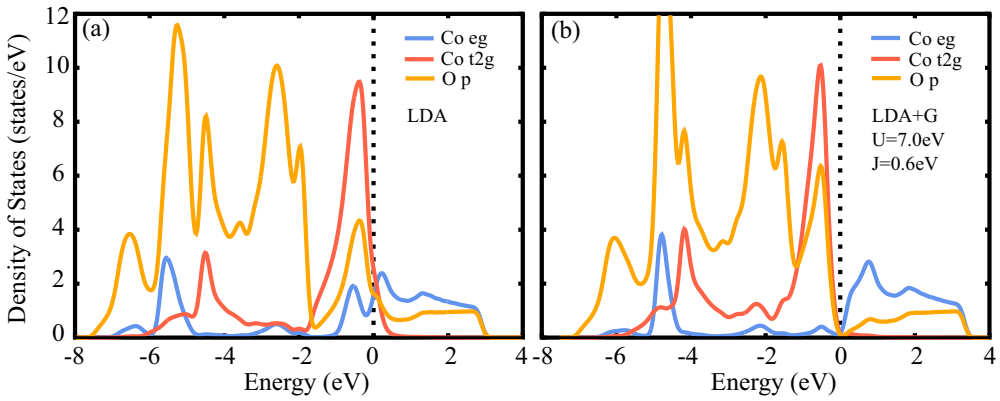

FIG. 2. (Color online) The partial density of states for total Co e_g, t_{2g} states and total O $2p$ states in one primitive cell of bulk $LaCoO_3$ for (a) LDA calculation and for (b) LDA+G calculation with $U = 7.0$ eV, $J = 0.6$ eV.

The LDA band structure with the optimized structure is then obtained and shown in Fig. 3(f), from which we can find two nearly flat bands with bandwidth being around 0.06 eV at the top and the bottom of the Co e_g bands. The most important difference between the electronic structure of the bulk material and heterostructure of $LaCoO_3$ is that the formal charge of Co $3d$ orbitals increases from 6 to 6.5 in the heterostructure. This is due to the fact that the (111) interface between $SrTiO_3$ and $LaCoO_3$ is polarized leading to one electron transfer from Ti to Co. As illustrated in Fig. 4, there is charge mismatch between one layer of Ti^{+4} and one layer of $(LaO_3)^{-3}$, Ti will lose four electrons, but LaO_3 can only accept three electrons, so there will be one electron left and will be transferred to the two layers of Co due to the conservation of total charge. We want to emphasize that this charge transfer is due to the electric polarization instead of the hybridization of bands. As a consequence, the bottom flat band crosses the Fermi level and is nearly half-filled. The TB model used for the further

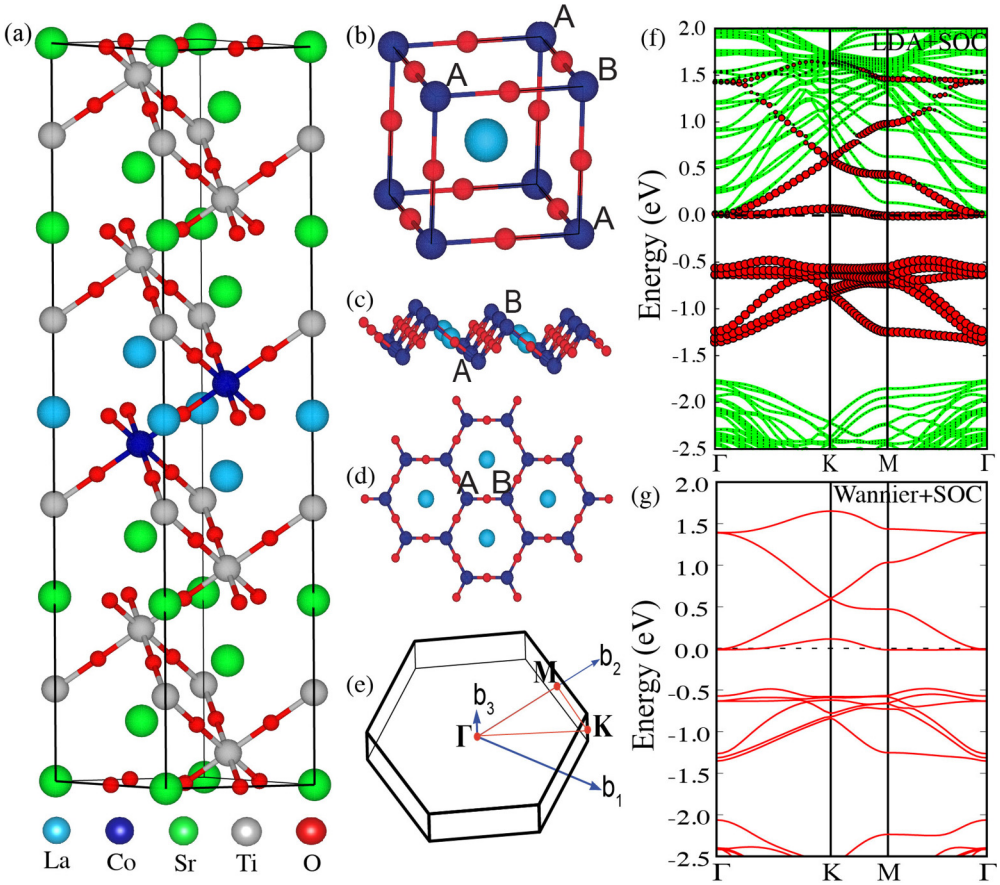

FIG. 3. (Color online) (a) The heterostructure of $LaCoO_3$, two layers of Co and three layers of LaO_3, are grown along the (111) direction on $SrTiO_3$. (b)–(d) Illustrate the formation of a buckled honeycomb lattice by two layers of TM ions along the (111) direction of an ideal perovskite lattice. (e) The Brillouin zone of the honeycomb lattice. (f) The fat bands derived from the LDA+SOC calculation and (g) the band structure obtained by the Wannier TB Hamiltonian.

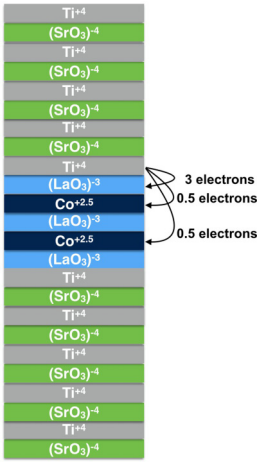

FIG. 4. (Color online) Illustration of the charge transfer from Ti to Co in the heterostructure of $LaCoO_3$.

study is then constructed in the following way. First, based on the non-SOC LDA calculations we construct a TB model containing 20 d orbitals (including spin degree of freedom) from two Co atoms and 54 p orbitals from the oxygen atoms in the three nearest layers. Then an atomic SOC Hamiltonian is added to the Hamiltonian in Eq. (1), which reads

$$H_{\mathrm{SOC}} = \lambda \sum_i \vec{\mathbf{l}}_i \cdot \vec{\mathbf{s}}_i, \tag{6}$$

where the strength $\lambda = 50$ meV is determined by fitting the LDA+SOC results.

The band structure without SOC shows a clear quadratic band touching at the Γ point, which is unstable against infinitesimally small Coulomb interaction if the chemical potential lies exactly at the touching point [52]. With SOC, the fourfold degenerate bands at Γ point split into two doubly degenerate bands by the second order effects of SOC. The splitting is around 7 meV in $LaCoO_3$, which can be hardly seen from Figs. 3(f) and 3(g). If the flat band is fully filled, the Berry phase structure generated by SOC around the Γ point makes it a two-dimensional topological insulator with the nontrivial Z_2 index. As mentioned above, in reality the flat band is only half-filled and the system will keep metallic in paramagnetic phase. While we have already seen in the bulk calculation, the correct semiconductorlike electronic states can only be obtained when the strong Coulomb interaction among the 3d electrons has been considered in a proper way. For the bilayer $LaCoO_3$ system, the Coulomb interaction has two important effects. First it greatly enhances the SOC, which stabilizes the topological phase. Secondly, it generates strong Stoner instability in the flat band and makes the ground state FM. When the FM exchange coupling overcomes the bandwidth of the flat band, the flat band will be completely polarized and an FM insulator phase is formed with the gap opening at the Γ point by correlation enhanced effective SOC. The nonmagnetic band structure is already Z_2 nontrivial; the spin up and down subsystems can be viewed as two Chern insulators with opposite Chern number -1 and 1. Therefore when it is completely polarized, it naturally leads to the Chern insulator phase with Chern number 1.

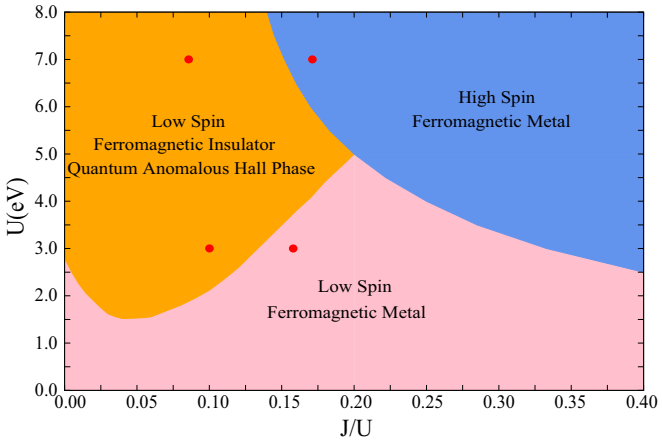

FIG. 5. (Color online) The phase diagram calculated by the LDA+G method in the plane of Coulomb interaction U and Hund's rule coupling J. There are three regions: (pink) low spin ferromagnetic metal (LS-FM-M), (orange) low spin ferromagnetic insulator (LS-FM-I), and (blue) high spin ferromagnetic metal (HS-FM-M).

We then apply the LDA+G method to carefully consider the Coulomb interaction. A phase diagram with both Coulomb interaction U and Hund's rule coupling J has been obtained as shown in Fig. 5. The phase diagram is obtained by searching for the ground state by LDA+G on a 40×40 uniform grid in the parameter space spanned by U and J/U. The spin state is determined by calculating $\langle G \mid S^2 \mid G \rangle$, where S^2 is the total spin operator. The semiconductor gap is determined by the energy difference between the bottom of the conduction band and the top of the valence band. The system is metallic when such a semiconductor gap becomes negative. Two typical Coulomb interaction strengths U have been chosen to plot their magnetization as a function of J/U, which is shown in Fig. 6, and four typical points (red circle) have been chosen to plot their quasiparticle band structures and the probability of the atomic configurations, as shown in Fig. 7. There are mainly three regions in the phase diagram: low spin ferromagnetic metal (LS-FM-M), low spin ferromagnetic insulator (LS-FM-I), and high spin ferromagnetic metal (HS-FM-M). The

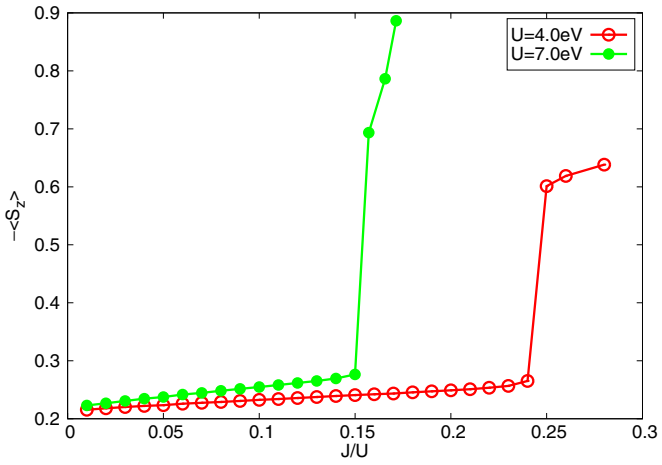

FIG. 6. (Color online) The magnetization of the ground state as the function of J/U for two different Hubbard U values.

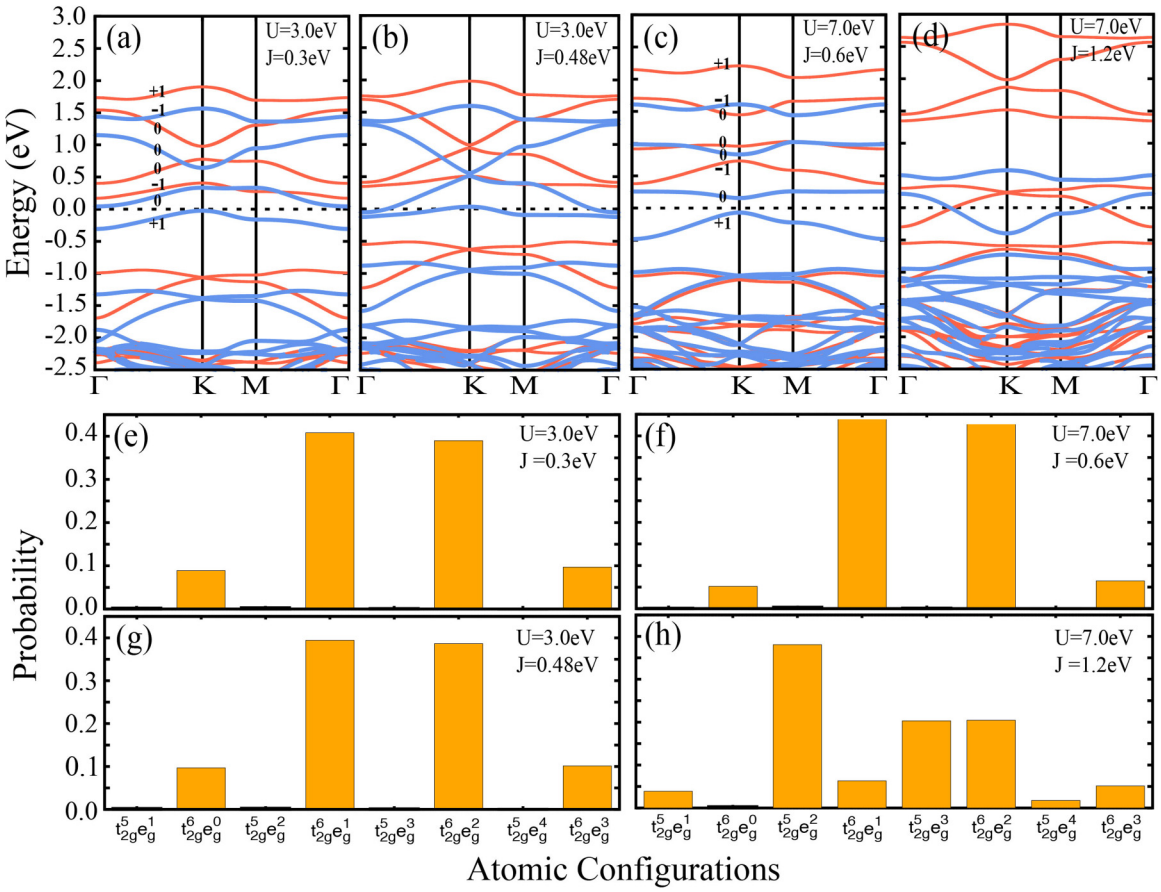

FIG. 7. (Color online) Four points are chosen from the phase diagram to plot their band structures and corresponding probability of the atomic configurations. (a)–(d) The Gutzwiller quasiparticle band structures; blue and red lines indicate the majority and minority bands, respectively; the numbers in (a) and (c) are the Chern numbers for separate bands. (e)–(h) The corresponding probability of the atomic configurations $|I\rangle$ in the Gutzwiller wave function $|G\rangle$ indicating the spin states.

Coulomb interaction is much larger than the bandwidth of the flat band; as a consequence, the FM order can be easily formed and stabilized according to the Stoner's criteria. As shown in Fig. 6, with the increment of Hund's rule coupling the FM polarization becomes stronger, and suddenly jumps at the phase boundary between LS phases and HS phases indicating the corresponding transition is first order. In comparison, we haven't found any stable AFM order in our calculations.

From the above discussion, we can draw a conclusion that the FM insulator phase can appear only when the following two conditions are satisfied: (i) the effective SOC is big enough to split the band touching point at the Γ point, (ii) the FM exchange coupling is big enough to make the flat band around the chemical potential fully polarized. As discussed previously, the interaction parameters for $LaCoO_3$ are around $U = 7.0$ eV and $J = 0.6$ eV, with which our LDA+G calculation obtains quite a robust FM insulator phase with Chern number 1. The corresponding quasiparticle band structure has been plotted in Fig. 7(c), where the semiconductor gap around 0.22 eV lying between two bands with majority spin. The appearance of semiconductor behavior is mainly due to the effective SOC, which is greatly enhanced by the strong correlation effects in $LaCoO_3$. In this system, the effective SOC in the e_g bands can be modified by the local correlation effects through two ways. The first effect is due to Hund's rule coupling J, which competes against the crystal field splitting between the e_g and t_{2g} bands and reduces the energy cost for virtual particle-hole excitations between them. Since the effective SOC in the e_g bands is a second order effect caused by such virtual excitations, the Hund's rule coupling can then enhance the effective SOC. The second effect is mainly due to the Coulomb interaction between different orbitals ($U' = U - 2J$), which also enhances the effective SOC [53,54] through the Hartree-Fock process especially when the SOC splitting is between one almost fully occupied level and one almost empty level. Although the Coulomb interaction is treated on the level of the Gutzwiller approximation, we believe that the main physics of the interaction enhanced SOC has been well captured. We note that the Gutzwiller approximation only becomes exact in infinite dimension, where only the local correlation needs to be considered. The nonlocal correlation in 2D will be expected to reduce both the semiconducting gap and the effective SOC. In the present study, the possible lattice distortion, which may also be enhanced by strong Coulomb interaction, has been neglected under the assumption that the pinning force from the substrate is strong enough to prevent it from happening. While in more realistic systems, the above assumption may not be well satisfied and further studies including the possible lattice distortion are needed, which will be discussed elsewhere.

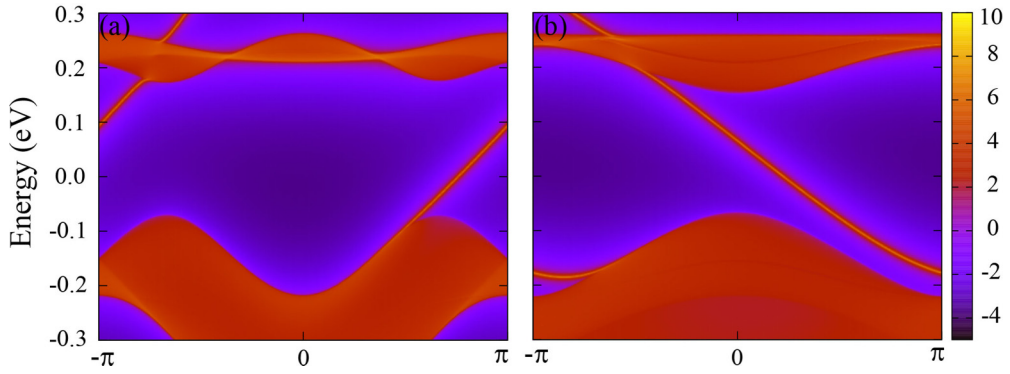

FIG. 8. (Color online) The local density of states for two identical edge modes of the buckled honeycomb lattice: (a) for zigzag edge and (b) for armchair edge.

As shown in Fig. 5, in most of the phase region, the favorable spin state of the bilayer $LaCoO_3$ system is the LS state. This is reasonable because the electron transfer induced by the charge mismatch increases the formal charge on Co $3d$ orbitals to be around 6.5, which further stabilizes the LS state compared with the bulk material. Without Hund's rule coupling the minimum Coulomb interaction strength required to open the semiconductor gap is around 3.0 eV, which is far below the actual parameter for $LaCoO_3$ (7.0 eV), indicating the robustness of the predicted QAH phase in this system. The increasing of Hund's rule coupling will first enhance the effective SOC by reducing the energy cost for the virtual particle-hole excitation between e_g and t_{2g} bands and favors the FM insulator phase. While when J/U is bigger than 0.05, further increasing J will dramatically reduce the effective SOC and favors the FM metal phase. This is due to the fact that the increment of J always comes together with the decrement of interorbital repulsion U' (equals $U - 2J$), which has the dominant effect on effective SOC in this phase region. With the actual Hubbard interaction $U = 7.0$ eV, the effective SOC is always very large when it is in the LS state; the FM insulator phase can only be destroyed by increasing the Hund's rule coupling J to induce a spin state transition from LS to HS states. As plotted in Fig. 7(d), when the HS state is stabilized by strong enough Hund's rule coupling, two of the t_{2g} bands are lifted across the Fermi level generating an FM metal phase. Therefore, the most important conclusion we can reach from the phase diagram is that with the reasonable U and J strength, as long as the LS state can be stabilized, the FM insulator phase with the nonzero Chern number is always robust.

With the effective quasiparticle Hamiltonian obtained by LDA+G, we have also calculated the Chern number by the Kubo formula [55] for the FM insulator phase, which equals 1 as we expected. The edge states along both zigzag and armchair types of edges are also calculated and plotted in Figs. 8(a) and 8(b), showing the typical chiral nature of the edge states in QAH states.

IV. SUMMARY

In summary, we have studied the strongly correlated (111) bilayer heterostructure of $LaCoO_3$ by the LDA+G method. Our results verify that Coulomb interactions can largely enhance the effective SOC and stabilize a very robust LS-FM-I state due to the strong stoner instability in the topologically nontrivial flat band. The calculated Chern number $C = 1$ and the edge states indicate a possible QAH effect in this system. Besides, the strong correlation between the spin state of Co and the low energy band structure provides another way to tune the topological properties. We believe that the fast development of the oxide MBE technique provides a great opportunity in this system to realize the QAH effect.

ACKNOWLEDGMENTS

We acknowledge the helpful discussions with Y. Ran and N. Nagaosa. This work was supported by the NSF of China and by the 973 program of China (Grants No. 2011CBA00108 and No. 2013CB921700). The calculations were preformed on TianHe-1(A), the National Supercomputer Center in Tianjin, China.

[1] M. Z. Hasan and C. L. Kane, Rev. Mod. Phys. **82**, 3045 (2010).
[2] X.-L. Qi and S.-C. Zhang, Rev. Mod. Phys. **83**, 1057 (2011).
[3] D. Xiao, W. Zhu, Y. Ran, N. Nagaosa, and S. Okamoto, Nat. Cummun. **2**, 596 (2011).
[4] B. A. Bernevig, T. L. Hughes, and S.-C. Zhang, Science **314**, 1757 (2006).
[5] M. König, S. Wiedmann, C. Brüne, A. Roth, H. Buhmann, L. W. Molenkamp, X.-L. Qi, and S.-C. Zhang, Science **318**, 766 (2007).
[6] X. Dai, T. L. Hughes, X.-L. Qi, Z. Fang, and S.-C. Zhang, Phys. Rev. B **77**, 125319 (2008).
[7] H. Zhang, C.-X. Liu, X.-L. Qi, X. Dai, Z. Fang, and S.-C. Zhang, Nat. Phys. **5**, 438 (2009).
[8] Y. Xia, D. Qian, D. Hsieh, L. Wray, A. Pal, H. Lin, A. Bansil, D. Grauer, Y. S. Hor, R. J. Cava, and M. Z. Hasan, Nat. Phys. **5**, 398 (2009).
[9] Y. L. Chen, J. G. Analytis, J.-H. Chu, Z. K. Liu, S.-K. Mo, X. L. Qi, H. J. Zhang, D. H. Lu, X. Dai, Z. Fang, S. C. Zhang, I. R. Fisher, Z. Hussain, and Z.-X. Shen, Science **325**, 178 (2009).

[10] M. Izumi, Y. Ogimoto, Y. Konishi, T. Manako, M. Kawasaki, and Y. Tokura, Mater. Sci. Eng. B **84**, 53 (2001).
[11] A. Ohtomo, D. A. Muller, J. L. Grazul, and H. Y. Hwang, Nature (London) **419**, 378 (2002).
[12] A. Ohtomo and H. Y. Hwang, Nature (London) **427**, 423 (2004).
[13] A. H. Castro Neto, F. Guinea, N. M. R. Peres, K. S. Novoselov, and A. K. Geim, Rev. Mod. Phys. **81**, 109 (2009).
[14] K.-Y. Yang, W. Zhu, D. Xiao, S. Okamoto, Z. Wang, and Y. Ran, Phys. Rev. B **84**, 201104 (2011).
[15] A. Rüegg and G. A. Fiete, Phys. Rev. B **84**, 201103 (2011).
[16] A. Rüegg, C. Mitra, A. A. Demkov, and G. A. Fiete, Phys. Rev. B **85**, 245131 (2012).
[17] A. Rüegg, C. Mitra, A. A. Demkov, and G. A. Fiete, Phys. Rev. B **88**, 115146 (2013).
[18] S. Middey, D. Meyers, D. Doennig, M. Kareev, X. Liu, Y. Cao, P. J. Ryan, R. Pentcheva, J. W. Freeland, and J. Chakhalian, arXiv:1407.1570.
[19] J. Bünemann, W. Weber, and F. Gebhard, Phys. Rev. B **57**, 6896 (1998).
[20] X. Deng, L. Wang, X. Dai, and Z. Fang, Phys. Rev. B **79**, 075114 (2009).
[21] N. Lanatà, H. U. R. Strand, X. Dai, and B. Hellsing, Phys. Rev. B **85**, 035133 (2012).
[22] F. Lu, J. Zhao, H. Weng, Z. Fang, and X. Dai, Phys. Rev. Lett. **110**, 096401 (2013).
[23] G. Kresse and J. Furthmüller, Phys. Rev. B **54**, 11169 (1996).
[24] P. E. Blöchl, Phys. Rev. B **50**, 17953 (1994).
[25] G. Kresse and D. Joubert, Phys. Rev. B **59**, 1758 (1999).
[26] J. P. Perdew, K. Burke, and M. Ernzerhof, Phys. Rev. Lett. **77**, 3865 (1996).
[27] N. Marzari, A. A. Mostofi, J. R. Yates, I. Souza, and D. Vanderbilt, Rev. Mod. Phys. **84**, 1419 (2012).
[28] A. A. Mostofi, J. R. Yates, Y.-S. Lee, I. Souza, D. Vanderbilt, and N. Marzari, Comput. Phys. Commun. **178**, 685 (2008).
[29] S. Sugano, Y. Tanabe, and H. Kamimura, *Multiplets of Transition-metal Ions in Crystals* (Academic Press, New York, 1970).
[30] A. Georges, L. D. Medici, and J. Mravlje, Annu. Rev. Condens. Matter Phys. **4**, 137 (2013).
[31] F. de Groot, J. Fuggle, B. Thole, and G. Sawatzky, Phys. Rev. B **42**, 5459 (1990).
[32] V. Anisimov and Y. Izyumov, *Electronic Structure of Strongly Correlated Materials* (Springer, Berlin/Heidelberg, 2010).
[33] M. Abbate, R. Potze, G. A. Sawatzky, and A. Fujimori, Phys. Rev. B **49**, 7210 (1994).
[34] M. A. Korotin, S. Y. Ezhov, I. V. Solovyev, V. I. Anisimov, D. I. Khomskii, and G. A. Sawatzky, Phys. Rev. B **54**, 5309 (1996).
[35] S. Yamaguchi, Y. Okimoto, and Y. Tokura, Phys. Rev. B **55**, R8666 (1997).
[36] K. Asai, A. Yoneda, O. Yokokura, J. Tranquada, G. Shirane, and K. Kohn, J. Phys. Soc. Jpn. **67**, 290 (1998).
[37] S. Yamaguchi, Y. Okimoto, H. Taniguchi, and Y. Tokura, Phys. Rev. B **53**, R2926 (1996).
[38] Y. Tokura, Y. Okimoto, S. Yamaguchi, H. Taniguchi, T. Kimura, and H. Takagi, Phys. Rev. B **58**, R1699 (1998).
[39] M. Imada, A. Fujimori, and Y. Tokura, Rev. Mod. Phys. **70**, 1039 (1998).
[40] P. G. Radaelli and S.-W. Cheong, Phys. Rev. B **66**, 094408 (2002).
[41] C. Zobel, M. Kriener, D. Bruns, J. Baier, M. Grüninger, T. Lorenz, P. Reutler, and A. Revcolevschi, Phys. Rev. B **66**, 020402 (2002).
[42] K. Knížek, P. Novák, and Z. Jirák, Phys. Rev. B **71**, 054420 (2005).
[43] M. W. Haverkort, Z. Hu, J. C. Cezar, T. Burnus, H. Hartmann, M. Reuther, C. Zobel, T. Lorenz, A. Tanaka, N. B. Brookes, H. H. Hsieh, H.-J. Lin, C. T. Chen, and L. H. Tjeng, Phys. Rev. Lett. **97**, 176405 (2006).
[44] R. F. Klie, J. C. Zheng, Y. Zhu, M. Varela, J. Wu, and C. Leighton, Phys. Rev. Lett. **99**, 047203 (2007).
[45] S. K. Pandey, A. Kumar, S. Patil, V. R. R. Medicherla, R. S. Singh, K. Maiti, D. Prabhakaran, A. T. Boothroyd, and A. V. Pimpale, Phys. Rev. B **77**, 045123 (2008).
[46] L. Craco and E. Müller-Hartmann, Phys. Rev. B **77**, 045130 (2008).
[47] H. Hsu, K. Umemoto, M. Cococcioni, and R. Wentzcovitch, Phys. Rev. B **79**, 125124 (2009).
[48] R. Eder, Phys. Rev. B **81**, 035101 (2010).
[49] J. Kuneš and V. Křápek, Phys. Rev. Lett. **106**, 256401 (2011).
[50] V. Křápek, P. Novák, J. Kuneš, D. Novoselov, D. M. Korotin, and V. I. Anisimov, Phys. Rev. B **86**, 195104 (2012).
[51] G. Zhang, E. Gorelov, E. Koch, and E. Pavarini, Phys. Rev. B **86**, 184413 (2012).
[52] K. Sun, H. Yao, E. Fradkin, and S. A. Kivelson, Phys. Rev. Lett. **103**, 046811 (2009).
[53] G.-Q. Liu, V. N. Antonov, O. Jepsen, and O. K. Andersen, Phys. Rev. Lett. **101**, 026408 (2008).
[54] L. Du, L. Huang, and X. Dai, Eur. Phys. J. B **86**, 1 (2013).
[55] N. Nagaosa, J. Sinova, S. Onoda, A. H. MacDonald, and N. P. Ong, Rev. Mod. Phys. **82**, 1539 (2010).